NANO LETTERS

Letter

pubs.acs.org/NanoLett

When Nanowires Meet Ultrahigh Ferroelectric Field–High-Performance Full-Depleted Nanowire Photodetectors

Dingshan Zheng,[†,‡] Jianlu Wang,[†] Weida Hu,[*,†] Lei Liao,[*,‡] Hehai Fang,[†] Nan Guo,[†] Peng Wang,[†] Fan Gong,[‡] Xudong Wang,[†] Zhiyong Fan,[§] Xing Wu,[‖] Xiangjian Meng,[†] Xiaoshuang Chen,[†] and Wei Lu[†]

[†]National Laboratory for Infrared Physics, Shanghai Institute of Technical Physics, Chinese Academy of Sciences, Shanghai 200083, China

[‡]Department of Physics and Key Laboratory of Artificial Micro- and Nano-structures of Ministry of Education, Wuhan University, Wuhan 430072, China

[§]Department of Electronic and Computer Engineering, Hong Kong University of Science and Technology, Hong Kong SAR, China

[‖]Key Laboratory of Polar Materials and Devices of MOE, East China Normal University, Shanghai 200241, China

Supporting Information

ABSTRACT: One-dimensional semiconductor nanowires (NWs) have been widely applied in photodetector due to their excellent optoelectronic characteristics. However, intrinsic carrier concentration at certain level results in appreciable dark current, which limits the detectivity of the devices. Here, we fabricated a novel type of ferroelectric-enhanced side-gated NW photodetectors. The intrinsic carriers in the NW channel can be fully depleted by the ultrahigh electrostatic field from polarization of P(VDF-TrFE) ferroelectric polymer. In this scenario, the dark current is significantly reduced and thus the sensitivity of the photodetector is increased even when the gate voltage is removed. Particularly, a single InP NW photodetector exhibits high-photoconductive gain of 4.2×10^5, responsivity of 2.8×10^5 A W^{-1}, and specific detectivity (D^*) of 9.1×10^{15} Jones at $\lambda = 830$ nm. To further demonstrate the universality of the configuration we also demonstrate ferroelectric polymer side-gated single CdS NW photodetectors with ultrahigh photoconductive gain of 1.2×10^7, responsivity of 5.2×10^6 A W^{-1} and D^* up to 1.7×10^{18} Jones at $\lambda = 520$ nm. Overall, our work demonstrates a new approach to fabricate a controllable, full-depleted, and high-performance NW photodetector. This can inspire novel device structure design of high-performance optoelectronic devices based on semiconductor NWs.

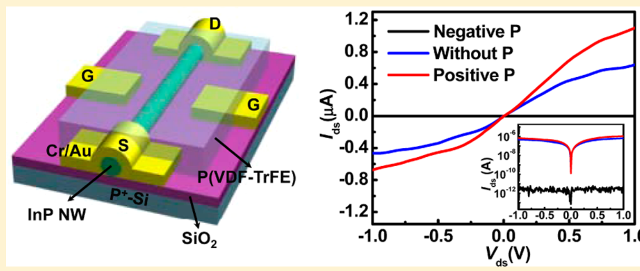

KEYWORDS: *Nanowire, photodetector, side-gated, photoresponsivity, ferroelectric polymer*

In recent years, one-dimensional semiconductor nanowires (NWs) have been regarded as potential building blocks for electronic and optoelectronic devices,[1] such as nanolasers,[2−4] light-emitting diodes,[5,6] solar cells,[7,8] gas and chemical sensors,[9−11] field emitters,[12,13] optical switches,[14,15] and photodetectors.[16−19] Among these applications, NW photodetectors have been realized with high photoconductive gain, controllable wavelength sensitivity, fast-response, and efficient light-to-current conversion for their desirable optoelectronic characteristics such as tunable light absorption and high carrier mobility.[20] However, it was found that the device performance is strongly suppressed by defect-induced intrinsic carriers and surface-trapped charges from their rich surface state, large surface-to-volume ratio, and high unintentional doping density.[16,20] Typically, when the NWs are used as photoconductive photodetectors or phototransistors, those intrinsic disadvantages lead to large dark current, thus lowering the ratio of light to dark current (I_{light}/I_{dark}), limiting detectivity of the photodetectors.

Recently, band-edge modulation schemes have been utilized to improve the photodetection performance of the device. For instance, supersensitive and fast-response optoelectronic devices have been realized using Schottky contact,[10,20−23] element doping,[24−26] and composition engineering.[8,27,28] As a typical direct band gap (1.34 eV) III−V semiconductor, indium phosphide (InP) NWs have demonstrated great potential in electronic and optoelectronic applications.[1,4,7,29−31] The rigid and flexible InP NWs photodetectors have been fabricated and exhibited a high photoresponsivity of 779.14 A W^{-1}.[29] Moreover, due to their remarkable optoelectronic characteristics in the visible light range cadmium sulfide (CdS) NWs and nanobelts (NBs) are also considered to be desirable materials for optoelectronic devices.[3,15,23,32−36] The CdS NB photodetectors exhibited an ultrahigh photoresponsivity of 7.3×10^4 A W^{-1}, which was the highest value among all the CdS

Received: January 8, 2016
Revised: February 26, 2016
Published: March 17, 2016

DOI: 10.1021/acs.nanolett.6b00104
Nano Lett. 2016, 16, 2548−2555

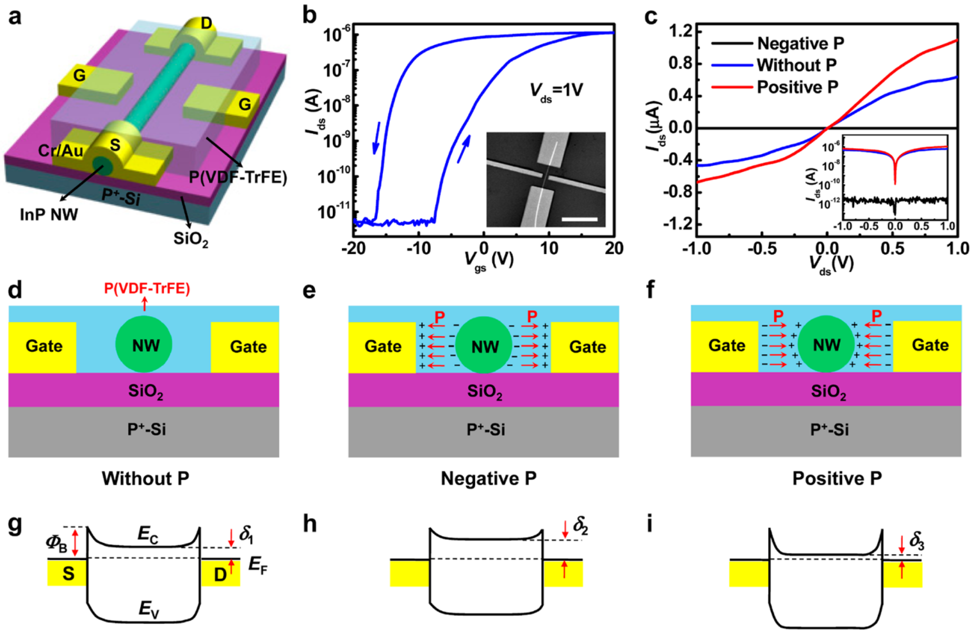

Figure 1. Schematic diagrams of ferroelectric side-gated single InP NW photodetector. (a) Three-dimensional schematic view of the ferroelectric side-gated single InP NW photodetector. (b) The transfer curves of InP NW FET with P(VDF-TrFE) ferroelectric polymer. The inset is the SEM image of InP NW FETs, the channel length (L) is 3.0 μm, the InP NW diameter (d) is 90 nm, and the distance between gate electrode and NW is 290 and 400 nm, respectively. The scale bar is 5 μm. (c) The I_{ds}−V_{ds} characteristics of three states without additional gate voltage. The three states are without polarization state (Without P), negative polarization state (Negative P) (polarized by a pulse V_{gs} of −20 V and the pulse width of 2 s), and positive polarization state (Positive P) (polarized by a pulse V_{gs} of +20 V and the pulse width of 2 s), respectively. (d−i) The schematic diagrams of the device and equilibrium energy band diagrams of three different ferroelectric polarization states at V_{ds} = 0 V. E_F is the Fermi level energy, E_C is the minimum conduction band energy, E_V is the maximum valence band energy, and Φ_B is the Schottky barrier height. δ is the height from bottom of conduction band to the Fermi level energy. δ_1, δ_2, and δ_3 are related to the three states, respectively.

photodetectors.[36] However, the detectivity of the device still needs improvement for its large dark current. Therefore, it is an urgent need to develop a unique device structure that can deplete the concentration of those defect/trap induced carriers and thus increase signal-to-noise ratio and detectivity of NW based photodetectors.

In this work, we design and fabricate ferroelectric polymer side-gated single NW photodetectors for the first time. With the ultrahigh ferroelectric polarization field of ferroelectric polymer, we achieve the full depletion of the intrinsic carriers in the NW channels, which significantly reduces the dark current and increases the sensitivity of the photodetectors even when the gate voltage is removed. Utilizing this device structure, a typical InP NW device exhibits the high photoconductive gain of 4.2 × 10^5, responsivity of 2.8 × 10^5 A $W^{-1,}$ and detectivity (D*) up to 9.1 × 10^{15} Jones, which are 2 orders of magnitude larger than that of commercially available Si, GaAs, or InGaAs photodetectors.[20,37−39] To further demonstrate the universality of the configuration for nanowires, we also demonstrate the ferroelectric polymer side-gated single CdS NW photodetector with a ultrahigher photoconductive gain of 1.2 × 10^7, responsivity of 5.2 × 10^6 A W^{-1}, and D* up to 1.7 × 10^{18} Jones.

The InP NWs were synthesized in a high-temperature tube furnace by chemical vapor deposition (CVD) method (see Supporting Information for details). The NWs were characterized by using scanning electron microscope (SEM), high-resolution transmission electron microscopy (HR-TEM), X-ray diffraction (XRD), and energy-dispersive X-ray spectroscopy (EDS) (see Supporting Information Figure S1). The results are consistent with the previous reports.[29] Single InP NW back-gated field-effect transistor (FET) was fabricated by electron-beam lithography (EBL), metal evaporation, and lift-off process. Moreover, the transfer and output characteristics of FET were measured at room temperature (see Supporting Information Figure S2 for details). There is a large current hysteresis window during V_{gs} sweeping, which is mainly originated from the surface species traps and can be explained by the electrons trapping and de-trapping process.[40] In addition, the optical and electronic properties of nanowire devices are strongly influenced by the surface defect state due to the large surface-to-volume ratio of NWs and the congregation of defects states near surfaces.[21,41] The electron mobility μ_{FE} of the single InP NW device can be calculated by using the expression of $\mu_{FE} = g_m L^2/(C_g V_{ds})$,[42] where the channel length L = 3.0 μm and $g_m = dI_{ds}/dV_{gs}$ is the transconductance of the NW device. C_g is the back gate capacitance that can be deduced based on the cylinder on-plane model:[42] $C_g = 2\pi\varepsilon_0\varepsilon_r L/[\ln(4h/d)]$, where ε_0 is permittivity of free space, ε_r is the dielectric constant of SiO_2, h = 110 nm is the thickness of the SiO_2 layer, and d = 90 nm is the InP NW diameter. The calculated carrier field-effect mobility is ~67.9 $cm^2\ V^{-1}\ s^{-1}$, which is comparable with the previous results.[29,43]

The photoresponse characteristics of InP NW photodetector were investigated at room temperature. Supporting Information Figure S2d presents the I_{ds}−V_{ds} characteristics of the InP NW photodetector in the dark and under illumination (830 nm, 55 mW cm^{-2}) at V_{gs} = 0 V. I_{dark} is the original current before the device was illuminated, and I_{light} is the current under light illumination. The net photocurrent, defined as $I_{ph} = |I_{light}| - |I_{dark}|$ = 0.42 μA is obtained at V_{gs} = 0 V and V_{ds} = 1 V. The device has a low I_{ph}/I_{dark} ratio (<1), which can be attributed to a large dark current. Therefore, in order to obtain a high ratio

DOI: 10.1021/acs.nanolett.6b00104
Nano Lett. 2016, 16, 2548−2555

of I_{ph}/I_{dark} and detectivity, it is necessary to suppress the dark current of the device.

The ferroelectric side-gated single InP NW photodetectors were fabricated and the device structure is schematically shown in Figure 1a. The side gate electrodes were fabricated as described above (see Methods for details). Additionally, a 200 nm of P(VDF-TrFE) (70:30 in mol %) film was spin-coated on the NWs channel. Then the P(VDF-TrFE) layer was annealed at 130 °C for 2 h on a hot plate to improve its crystallinity. A typical hysteresis loop of P(VDF-TrFE) capacitor was measured (see Supporting Information Figure S3). The coercive voltage is ~22.8 V and the remnant polarization value P_r is 7 μC cm^{-2}, indicating that the ferroelectric polymer has good polarization properties. The I_{ds}−V_{gs} transfer characteristics of the InP NW FET with ferroelectric polymer were acquired at room temperature, as shown in Figure 1b. Notably, the hysteresis loop of NW ferroelectric polymer side-gated device is traversed in a counterclockwise direction, which is in opposite to the typical clockwise hysteresis of NW back-gated device, demonstrating that the polarization of P(VDF-TrFE) film has a strong effect on the transfer characteristics of our devices.[44] The hysteresis window of ~10 V is caused by the polarization of the ferroelectric layer, when V_{gs} sweep range chosen from −20 V to +20 V at V_{ds} = 1 V. The device displays a high I_{on}/I_{off} ratio of 10^6 with the low off current of ~10^{-12} A. When a negative gate voltage of less than −16.6 V is applied, an off state is obtained, thus the dark current is suppressed due to the remnant polarization of the ferroelectric polymer. To further study the gated-bias-dependent behavior of the hysteresis, the transfer characteristic of the side-gated InP NW FET with P(VDF-TrFE) for different V_{gs} sweep ranges are measured (see Supporting Information Figure S4a). The results show that the hysteresis window becomes wider with the increase of the V_{gs} sweep range and the dark current is suppressed; both are due to the polarization of the ferroelectric layer.[45] In addition, studies on the gate-controlled characteristics of two different distances between gate electrode and NW have also been performed (see Supporting Information Figure S4b). The device with small distance shows a larger turn-on current and a positive shift of the threshold voltage, which can be attributed to the polarization of the ferroelectric layer.

In our work, the following three different scenarios are achieved for InP NW ferroelectric polymer side-gated structure: P(VDF-TrFE) without polarization state (Figure 1d), negative polarization state (Figure 1e), and positive polarization state (Figure 1f). The positive and negative polarization states were achieved by poling P(VDF-TrFE) with the gate bias of ±20 V and the pulse width of 2 s. When a negative V_{gs} pulse of 2 s is employed to one gate electrode, the polarization of the ferroelectric film will be aligned to this gate electrode under the negative electrostatic field gradient. On the contrary, the polarization of the ferroelectric film will be aligned to the NW. The I_{ds}−V_{ds} characteristics of the three scenarios are shown in Figure 1c, without additional gate voltage and light illumination. In the negative polarization state, I_{ds} is reduced to the noise current ~10^{-12} A. The electrostatic field derived from the remnant polarization of P(VDF-TrFE) after the application of a negative gate voltage, resulting in depletion of the electrons of the n-typed InP NW. Here, we can achieve the depletion of the intrinsic carriers with one gate electrode, as shown in Supporting Information Figure S5a. On the contrary, the positive polarization state corresponds to the accumulated states of carriers in the InP NW. The schematic diagrams of the device and equilibrium energy band diagrams of three different states are shown in Figure 1d−f and Figure 1g−i, respectively. In addition, the retention properties of the negative polarization and positive polarization states were measured (see Supporting Information Figure S5b). The device demonstrates stable retention characteristics (over 30 000 s) at room temperature. After the gate voltage pulse is removed, the device can still keep the working state of polarization induced by the remnant polarization of the ferroelectric polymer, indicating that our devices can work without additional gate voltage.

Figure 2a presents the I_{ds}−V_{ds} characteristics of ferroelectric polymer side-gated single InP NW photodetector measured in the dark and under illumination (830 nm, 55 mW cm^{-2}) without polarization. It is found that the net photocurrent I_{ph} = 0.45 μA is obtained at V_{ds} = 1 V without additional gate voltage. The device shows a very low ratio of I_{ph}/I_{dark} (~1), which is very close to the photocurrent of back-gated photodetector as measured above. However, I_{light} and I_{dark} are smaller than those of the back-gated device, which may be associated with the interface nature at the contacts.[46,47] Figure 2b shows the I_{ds}−V_{ds} characteristics of photodetector measured in the dark and under illumination after negative polarization process. I_{dark} is reduced to ~8 × 10^{-12} A, as the result of full depletion of carriers by the strong polarization of P(VDF-TrFE). Despite I_{light} decreasing slightly, the larger net photocurrent I_{ph} = 0.92 μA and a high ratio of I_{ph}/I_{dark} ~ 10^5 are obtained at V_{ds} = 1 V without additional gate voltage. The results indicate that the electrostatic field produced by the charge at the domain interface of P(VDF-TrFE) is strong enough to cause a full depletion of carriers in the InP NW semiconductor channel.[47] The photoresponse behavior of the photodetector can be explained by the energy band diagrams as shown in Figure 2c−f. In the positive polarization and without polarization states, both thermionic/tunneling currents and photon-generated current contribute to the channel current,[48] I_{light} = 1.09 μA. While in the negative polarization state, a full depletion of the intrinsic carriers is achieved in the NW channel, the photon-generated current dominants channel current,[48] and thus the

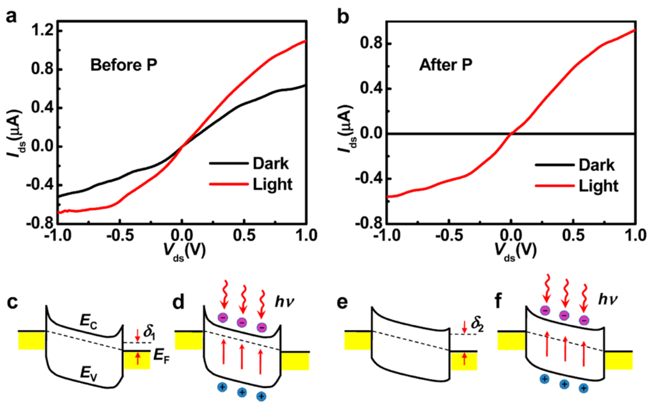

Figure 2. Ferroelectric-enhanced photoresponse of the ferroelectric side-gated single InP NW photodetector. (a) I_{ds}−V_{ds} characteristics of the photodetector in the dark and under illumination (830 nm, 55 mW cm^{-2}) without additional negative gate voltage. (b) I_{ds}−V_{ds} characteristics of photodetector in the dark and under illumination after negative polarization process. The energy band diagrams of different states under a drain−source bias in the dark and under illumination before negative polarization (c,d) and after negative polarization (e,f).

DOI: 10.1021/acs.nanolett.6b00104
Nano Lett. 2016, 16, 2548−2555

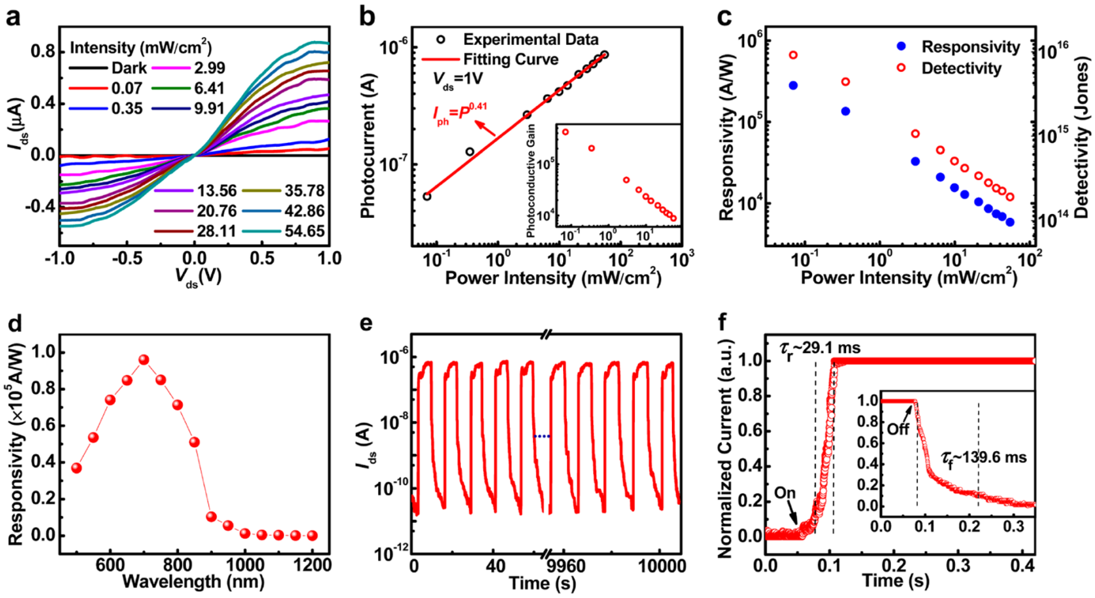

Figure 3. Photoresponse properties of the ferroelectric side-gated single InP NW photodetector. (a) I_{ds}−V_{ds} characteristics of the photodetector in the dark and under different light intensities (830 nm) after the device was depleted in the negative polarization state. (b) Dependence of photocurrent and photoconductive gain (the inset) on illumination power intensities. (c) Photoresponsivity and detectivity of the photodetector, showing high sensitivity. The device exhibits a responsivity of 2.8×10^5 A W^{-1}, and the detectivity is up to 9.1×10^{15} Jones under the low light intensity 0.07 mW cm^{-2}. (d) The responsivity of the detector under different illumination wavelengths from 500 to 1200 nm at a bias of 1 V (0.64 mW cm^{-2}). (e) Photocurrent response of the device, the laser light is turned on/off at an interval of 5 s (830 nm, 55 mW cm^{-2}) at V_{ds} = 1 V. (f) Time-resolved photoresponse of the device, the rise and fall of the photocurrent, and the fitted data using exponential functions at V_{ds} = 1 V.

light current decreases slightly, I_{light} = 0.92 μA. The dark current is reduced significantly after negative polarization, resulting in a high ratio of I_{ph}/I_{dark}.

To perform more systematic investigation, the ferroelectric polarization in P(VDF-TrFE) was preset at a negative polarization state by a short gate voltage pulse of −20 V on the side gate. Figure 3a presents the I_{ds}−V_{ds} characteristics for different light intensities at a wavelength of 830 nm after being depleted in the negative polarization state. The I_{ds}−V_{ds} curve shows a linear regime at low V_{ds} and a saturation regime at high V_{ds}. The saturation photocurrent may be affected by light intensity, the carrier density and light absorption efficiency, the interface crystallography, and the bias.[49,50] When the bias is large enough, there will be photon-generated carrier saturation and electron−hole recombination under strong light illumination.[17,51] As shown in Figure 3b, the relationship between photocurrent and light intensity obeys the power law[14,17] $I = cP^k$, where I is the photocurrent, c is a proportionality constant, P is the light intensity, and k is an empirical value. Through nonlinear fitting, we can obtain c = 1.7 and k = 0.41, depending on the complex processes of electron−hole generation, trapping, and recombination.[14,17] The I_{ph}/I_{dark} ratio under different light power intensities is shown in Supporting Information Figure S5c.

The photoconductive gain (G) is a key parameter to evaluate the sensitivity of nanoscaled photodetectors, which is defined as the ratio between the number of charges collected by the electrodes per unit time and the number of photons absorbed by the NW per unit time ($G = N_e/N_{ph}$).[51] The photoconductive gain can be expressed as[16,51,52] $G = (I_{ph}/e)/(PA/h\nu)$, where I_{ph} is the photocurrent, P is the incident power density, A is the effective irradiated area on the NW, $h\nu$ is the energy of an incident photon, and e is the electronic charge. Note that the cross-sectional area of the NW, $A = L \times d$ is an estimation of the effective irradiated area (L is the channel length, d is the NW diameter). To further confirm the absorption cross section of the NW, the simulation was carried out using the finite-difference time-domain (FDTD) method (see Supporting Information Figure S6 for details). It is found that the effective irradiated area of the simulation is comparable to the values used in the experiment. The inset of Figure 3b presents the calculated photoconductive gain for different power intensities. The G of the photodetector is up to 4.2×10^5 under the low light intensity of 0.07 mW cm^{-2}, due to the long photon-generated carrier lifetime in the NW compared to the short carrier transit time between the electrodes.[51,52] High gain indicates that large photocurrent output signals can be achieved with relatively low optical input.[16] The gain decreases with the increasing light intensity, which is a result of the carrier-trap saturation.[51]

The responsivity (R) and the detectivity (D^*) are also two key parameters for a photodetector.[53] The responsivity of a photodetector can be defined as[16,21,47] $R = I_{ph}/(PA)$, where I_{ph} is the photocurrent, P is the incident power density, and A is the effective irradiated area on the NW. In addition, the specific detectivity is an important figure-of-merit characterizing the capability of the smallest detectable signal for a photodetector, which can be defined as[16,37] $D^* = (A\Delta f)^{1/2}/(\mathrm{NEP})$, where A is the effective area of the detector, Δf is the electrical bandwidth in Hz, and NEP is the noise equivalent power. Considering the shot noise from dark current is the major factor limiting the detectivity, the specific detectivity can be expressed as[16,37,47] $D^* = RA^{1/2}/(2eI_{dark})^{1/2}$, where R is the responsivity, A is the effective area of the detector, e is the electronic charge, and I_{dark} is the dark current. Note that before being depleted, the R and D^* of the device are calculated as 3.1×10^3 A W^{-1} and 3.5×10^{11} Jones (under the high light intensity of 55 mW cm^{-2}), respectively (see Figure 2a). However, after being depleted, the

DOI: 10.1021/acs.nanolett.6b00104
Nano Lett. 2016, 16, 2548−2555

Table 1. Comparison of the Critical Parameters for Various Nanostructure Photodetectors at Visible and near Infrared Wavelength (NW, Nanowire; NB, Nanobelt; NR, Nanoribbon)

material	I_{on}/I_{off}	response time	recovery time	gain	responsivity (A W^{-1})	detectivity (Jones)	reference
commercial Si					300	$\sim 10^{13}$	37, 38
commercial GaAs					0.45		39
commercial InGaAs						$\sim 10^{12}$	37, 38
Si NW	3.5			10^5	2.56×10^4	$\sim 10^{13}$	52
GaAs/AlGaAs NW	10^2				0.57	7.2×10^{10}	20
InP NW	11	0.1 s	0.46 s		779.14		29
InAs NW	10^2				4.4×10^3	2.6×10^{11}	18
CdS NW	10^2	15 ms	15 ms				54
CdS NW	200	0.8 ms	240 ms				32
CdS NB	6	20 μs			7.3×10^4		36
CdS_xSe_{1-x} NR	10^6	30 ms	90 ms		1.16×10^3		28
InP NW	10^5	29.1 ms	139.6 ms	4.2×10^5	2.8×10^5	9.1×10^{15}	this work
CdS NW	10^7	17.2 ms	160.2 ms	1.2×10^7	5.2×10^6	1.7×10^{18}	this work

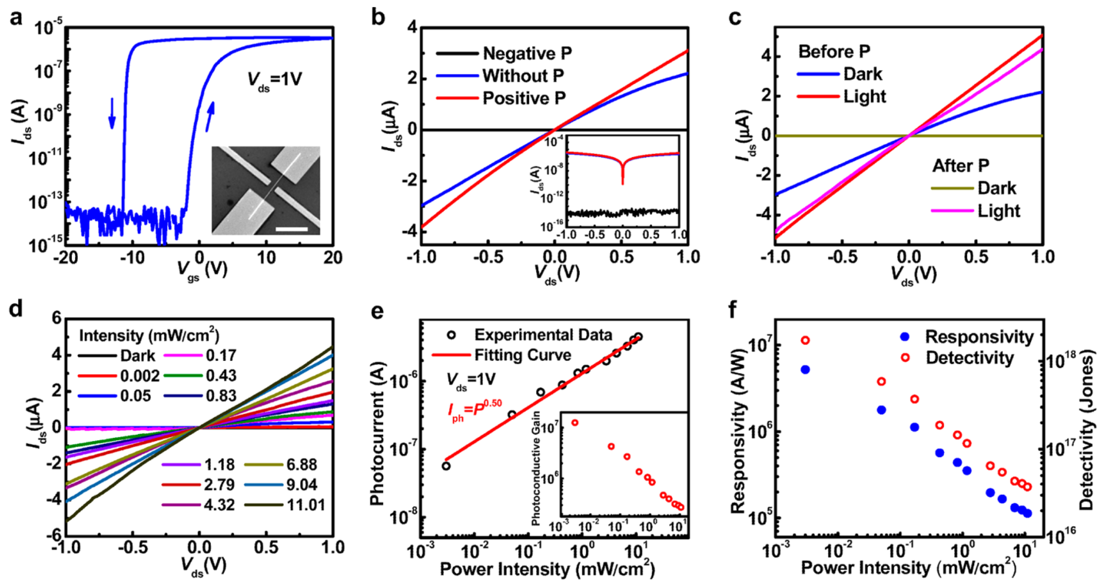

Figure 4. Electrical and photoresponse properties of the ferroelectric side-gated single CdS NW photodetector. (a) The transfer curves of CdS NW FET with P(VDF-TrFE) ferroelectric polymer. The inset is the SEM image of side-gated CdS NW FETs. The scale bar is 3 μm. (b) The $I_{ds}-V_{ds}$ characteristics of three states without light illumination and additional gate voltage. (c) $I_{ds}-V_{ds}$ characteristics of the photodetector in the dark and under illumination (520 nm, 11 mW cm^{-2}) before and after negative polarization. (d) $I_{ds}-V_{ds}$ characteristics of the CdS NW photodetector in the dark and under different light intensities (520 nm) after the device was depleted in the negative polarization state. (e) Dependence of photocurrent and photoconductive gain (the inset) on light intensities. (f) Photoresponsivity and detectivity of the CdS NW photodetector. The R and D^* of the photodetector are up to 5.2×10^6 A W^{-1} and 1.7×10^{18} Jones, respectively, under the low light intensity 0.003 mW cm^{-2}.

R and D^* of the device have been significantly improved to 6.2×10^3 A W^{-1} and 2.0×10^{14} Jones (under the high light intensity of 55 mW cm^{-2}), respectively (see Figure 2b). The D^* of the fully depleted device is ~500 times larger than that of the not depleted device, which is attributed to the much lower dark current of 8×10^{-12} A. Figure 3c presents the calculated values of responsivity and detectivity at different power intensities. It shows that R and D^* increase dramatically with the decreasing light intensity, and the R and D^* of the photodetector are up to 2.8×10^5 A W^{-1} and 9.1×10^{15} Jones, respectively, under the low light intensity of 0.07 mW cm^{-2}. The highest R and D^* are 2 orders of magnitude larger than that of the commercially available Si, GaAs, or InGaAs photodetectors.[20,37−39] Overall, we have achieved the full depletion of the intrinsic carriers in the NW channel with the ferroelectric polarization field of P(VDF-TrFE), which significantly reduces the dark current of the device. Low dark current, high photoconductive gain and responsivity, lead to detectivity of photodetector as high as 9.1×10^{15} Jones. The obtained R and D^* show better performance compared with those reported detectors at visible and near-infrared wavelength, as is shown in Table 1.

Figure 3d depicts the spectral response of the detector at different illumination wavelengths from 500 to 1200 nm at a bias of 1 V (under light intensity of 0.64 mW cm^{-2}). It is found that responsivity is the highest at around 700 nm and it sharply declines for the wavelength longer than 850 nm. While there is still appreciable photoresponse at 1000 nm, which is slightly longer than 925 nm (corresponding to InP band gap 1.34 eV). The slight increase of the cutoff wavelength can be ascribed to defects induced by the electrostatic fields from the ferroelectrics.[47]

To further investigate the response speed of our NW detector, time-resolved photoresponse measurements were

DOI: 10.1021/acs.nanolett.6b00104
Nano Lett. 2016, 16, 2548−2555

performed by periodically turning on and off the laser light (830 nm, 55 mW cm^{-2}). A high speed oscilloscope was used to monitor the fast-varying optical signal.[17] As shown in Figure 3e, the photodetector exhibits the excellent stability and reliability with the on/off photoswitching behavior at V_{ds} = 1 V without additional gate voltage. The response time (rise time τ_r), defined as the time for the photocurrent to increase from 10% I_{peak} to 90% I_{peak}, is 29.1 ms, and the recovery time (fall time τ_f), defined similarly, is 139.6 ms, as shown in Figure 3f. The longer recovery time may be related to the influence of surface states and/or the quality of the crystals.[17,48,55] Furthermore, the recombination of electrons and holes may be affected by the surface trap state of NW and the interface state between the NW and P(VDF-TrFE).[47] The time-resolved photoresponse measurement of a nonpolarized detector at V_{ds} = 1 V is shown in Supporting Information Figure S7a. In addition, Supporting Information Figure S7b presents the response to the limited fluorescent lighting (low light intensity of ~0.01 mW cm^{-2}) after negative polarization, confirming the ultrahigh sensitivity of the ferroelectric-enhanced side-gated InP NW photodetectors.

To further demonstrate the universality of our device configuration, ferroelectric side-gated single CdS NW photodetector has also been successfully fabricated and characterized, as shown in Figure 4. The characterizations of the as-grown CdS NWs are shown in Supporting Information Figure S8. The optoelectronic measurements of the back-gated CdS NW FETs were performed and shown in Supporting Information Figure S9. The CdS NW channel length L = 3.0 μm and diameter d = 120 nm (inset). The device displays a high I_{on}/I_{off} ratio of 10^7, and the calculated carrier field-effect mobility is ~112 $cm^2 V^{-1} s^{-1}$, which is comparable with previous results.[3,56,57] The net photocurrent I_{ph} = 3.0 μA is obtained at V_{gs} = 0 V and V_{ds} = 1 V (520 nm, 11 mW cm^{-2}). Apparently, the device has a very low ratio of I_{ph}/I_{dark} (~1), indicating that the large dark current limits the performance of the NW photodetector.

To suppress the dark current, the ferroelectric side-gated single CdS NW photodetector was fabricated. The $I_{ds}-V_{gs}$ transfer characteristics of the CdS NW FET with ferroelectric polymer were investigated at room temperature, as shown in Figure 4a. The corresponding hysteretic behaviors of the device are shown in Supporting Information Figure S10. The $I_{ds}-V_{ds}$ characteristics of three states are shown in Figure 4b without light illumination and additional gate voltage. In the negative polarization state, I_{ds} is reduced to the noise current ~1 × 10^{-13} A. The retention properties of the negative polarization and positive polarization states were measured (Supporting Information Figure S11a). Figure 4c presents the $I_{ds}-V_{ds}$ characteristics of CdS NW photodetector measured in the dark and under illumination (520 nm, 11 mW cm^{-2}) before and after negative polarization. Before the device was depleted, the net photocurrent I_{ph} = 2.9 μA, the responsivity R = 7.2 × 10^4 A W^{-1}, and the detectivity D^* = 5.2 × 10^{12} Jones were obtained. However, after the device was depleted I_{ph} = 4.4 μA, R = 1.1 × 10^5 A W^{-1}, and D^* = 8.2 × 10^{16} Jones were obtained. The D^* of the depleted device is ~10^4 times larger than that of the not depleted device. Figure 4d presents the $I_{ds}-V_{ds}$ characteristics for different power intensities at a wavelength of 520 nm after being depleted. The I_{ph}/I_{dark} ratio under different light power intensities is showed in Supporting Information Figure S11b. The dependence between photocurrent and light intensity can be obtained with the power law as $I = 1.3P^{0.50}$ (Figure 4e). The inset of Figure 4e presents the photoconductive gain for different light intensity. The gain G is up to 1.2 × 10^7 under the low light intensity of 0.003 mW cm^{-2}. As shown in Figure 4f, the calculated values of responsivity and detectivity at different power intensities have been achieved, the R and D^* of the photodetector are up to 5.2 × 10^6 A W^{-1} and 1.7 × 10^{18} Jones, respectively.

Figure 5a depicts the spectral response of the CdS NW photodetector for wavelengths range of 350−700 nm at a source-drain bias of 1 V (0.04 mW cm^{-2}). The responsivity is the highest at around 475 nm. And there is still appreciable photoresponse at 600 nm, which is slightly longer than 516 nm (corresponding to CdS band gap 2.4 eV). Time-resolved photoresponse measurements were performed (520 nm, 11 mW cm^{-2}), as shown in Figure 5b,c. The response time τ_r and the recovery time τ_f of the detector are about 17.2 and 160.2 ms, respectively. The time-resolved photoresponse measurement of a nonpolarized photodetector is shown in Supporting Information Figure S12. Due to the high detectivity achieved in our ferroelectric side-gated CdS NW photodetector, it may be suitable for the detection of weak signals, which has broad applications. Figure 5d presents the response under several kinds of typical weak signal, where the photocurrent reached approximately 1 μA under the illuminations of a lighter, electric torch, and limited fluorescent lighting. Obviously, the ferroelectric CdS NW photodetector is extremely sensitive to the weak signal.

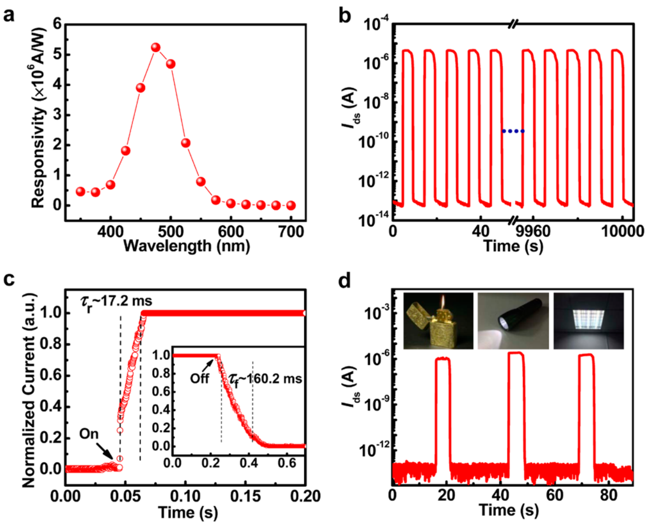

Figure 5. Spectral and time response characterizations of the ferroelectric side-gated single CdS NW photodetector. (a) The photoresponsivity of the detector under different illumination wavelengths from 350 to 700 nm at a bias of 1 V (0.04 mW cm^{-2}). (b) Photocurrent response of the device, the laser light is turned on/off at an interval of 5 s (520 nm, 11 mW cm^{-2}) at V_{ds} = 1 V. (c) Time-resolved photoresponse of the device, the rise and fall of the photocurrent and the fitted data using exponential functions, at V_{ds} = 1 V. (d) The photoresponse properties of photodetector under the illuminations of a lighter, electric torch, and limited fluorescent lighting, respectively, at V_{ds} = 1 V after negative polarization.

In summary, we have fabricated the ferroelectric polymer side-gated single NW photodetectors. The significant dark-current suppression is achieved by full carrier depletion caused by the inherent electric field from ferroelectric polarization of P(VDF-TrFE). The ferroelectric polymer side-gated single InP and CdS NW photodetectors exhibited ultrahigh detection

DOI: 10.1021/acs.nanolett.6b00104
Nano Lett. 2016, 16, 2548−2555

performance compared to traditional FET photodetectors. Particularly, the InP NW photodetector exhibits high photoconductive gain of 4.2×10^5, responsivity of 2.8×10^5 A W^{-1}, and high detectivity of 9.1×10^{15} Jones. Also, the CdS NW photodetector exhibits even higher photoconductive gain of 1.2×10^7, responsivity of 5.2×10^6 A W^{-1}, and detectivity of 1.7×10^{18} Jones, which are higher than any previous report for NWs photodetectors to our best knowledge. These results demonstrate a new generic device structure design that can lead to controllable, full-depleted, and high-performance NW photodetectors for a broad application.

■ ASSOCIATED CONTENT

Ⓢ Supporting Information

The Supporting Information is available free of charge on the ACS Publications website at DOI: 10.1021/acs.nanolett.6b00104.

Experimental procedure (nanowires synthesis, characterizations, photodetectors fabrication), simulation details, and figures (Figure S1–S12). (PDF)

■ AUTHOR INFORMATION

Corresponding Authors

*(W.H.) E-mail: wdhu@mail.sitp.ac.cn.
*(L.L.) E-mail: liaolei@whu.edu.cn.

Author Contributions

D.Z and J.W contributed equally to this work. W.H and L.L conceived and supervised the research. D.Z did the nanowire growth. D.Z and P.W fabricated the devices. D.Z, H.F, and P.W performed the measurements. H.F carried out the FDTD simulations. W.H, L.L, J.W, Z.F., and D.Z wrote the paper. X.W conducted the HR-TEM and verified the crystal structure. All authors discussed the results and revised the manuscript.

Notes

The authors declare no competing financial interest.

■ ACKNOWLEDGMENTS

This work was partially supported by the Major State Basic Research Development Program (Grant 2014CB921600), Natural Science Foundation of China (Grants 11322441, 61290301, 61574101, and 61574152), Fund of Shanghai Science and Technology Foundation (Grant 14JC1406400), CAS Interdisciplinary Innovation Team, and Ten Thousand Talents Program for Young Talents.

■ REFERENCES

(1) Duan, X. F.; Huang, Y.; Cui, Y.; Wang, J. F.; Lieber, C. M. *Nature* **2001**, *409*, 66–69.

(2) Huang, M. H.; Mao, S.; Feick, H.; Yan, H. Q.; Wu, Y. Y.; Kind, H.; Weber, E.; Russo, R.; Yang, P. D. *Science* **2001**, *292*, 1897–1899.

(3) Duan, X. F.; Huang, Y.; Agarwal, R.; Lieber, C. M. *Nature* **2003**, *421*, 241–245.

(4) Saxena, D.; Wang, F.; Gao, Q.; Mokkapati, S.; Tan, H. H.; Jagadish, C. *Nano Lett.* **2015**, *15*, 5342–8.

(5) Gudiksen, M. S.; Lauhon, L. J.; Wang, J.; Smith, D. C.; Lieber, C. M. *Nature* **2002**, *415*, 617–620.

(6) Tomioka, K.; Motohisa, J.; Hara, S.; Hiruma, K.; Fukui, T. *Nano Lett.* **2010**, *10* (5), 1639–44.

(7) Wallentin, J.; Anttu, N.; Asoli, D.; Huffman, M.; Aberg, I.; Magnusson, M. H.; Siefer, G.; Fuss-Kailuweit, P.; Dimroth, F.; Witzigmann, B.; Xu, H. Q.; Samuelson, L.; Deppert, K.; Borgstrom, M. T. *Science* **2013**, *339*, 1057–60.

(8) Li, L.; Lu, H.; Yang, Z.; Tong, L.; Bando, Y.; Golberg, D. *Adv. Mater.* **2013**, *25*, 1109–13.

(9) Zou, X.; Wang, J.; Liu, X.; Wang, C.; Jiang, Y.; Wang, Y.; Xiao, X.; Ho, J. C.; Li, J.; Jiang, C.; Fang, Y.; Liu, W.; Liao, L. *Nano Lett.* **2013**, *13*, 3287–92.

(10) Hu, Y.; Zhou, J.; Yeh, P. H.; Li, Z.; Wei, T. Y.; Wang, Z. L. *Adv. Mater.* **2010**, *22*, 3327–32.

(11) Liu, H.; Kameoka, J.; Czaplewski, D. A.; Craighead, H. G. *Nano Lett.* **2004**, *4*, 671–675.

(12) Chen, Z. G.; Cheng, L.; Zou, J.; Yao, X.; Lu, G. Q.; Cheng, H. M. *Nanotechnology* **2010**, *21*, 065701.

(13) Chen, Z. G.; Cheng, L.; Xu, H. Y.; Liu, J. Z.; Zou, J.; Sekiguchi, T.; Lu, G. Q.; Cheng, H. M. *Adv. Mater.* **2010**, *22*, 2376–80.

(14) Kind, H.; Yan, H. Q.; Messer, B.; Law, M.; Yang, P. D. *Adv. Mater.* **2002**, *14*, 158–160.

(15) Piccione, B.; Cho, C. H.; van Vugt, L. K.; Agarwal, R. *Nat. Nanotechnol.* **2012**, *7*, 640–645.

(16) Liu, X.; Gu, L.; Zhang, Q.; Wu, J.; Long, Y.; Fan, Z. *Nat. Commun.* **2014**, *5*, 4007.

(17) Guo, N.; Hu, W.; Liao, L.; Yip, S.; Ho, J. C.; Miao, J.; Zhang, Z.; Zou, J.; Jiang, T.; Wu, S.; Chen, X.; Lu, W. *Adv. Mater.* **2014**, *26*, 8203–9.

(18) Liu, Z.; Luo, T.; Liang, B.; Chen, G.; Yu, G.; Xie, X.; Chen, D.; Shen, G. *Nano Res.* **2013**, *6*, 775–783.

(19) Peng, K.; Parkinson, P.; Fu, L.; Gao, Q.; Jiang, N.; Guo, Y. N.; Wang, F.; Joyce, H. J.; Boland, J. L.; Tan, H. H.; Jagadish, C.; Johnston, M. B. *Nano Lett.* **2015**, *15*, 206–10.

(20) Dai, X.; Zhang, S.; Wang, Z.; Adamo, G.; Liu, H.; Huang, Y.; Couteau, C.; Soci, C. *Nano Lett.* **2014**, *14*, 2688–93.

(21) Miao, J. S.; Hu, W. D.; Guo, N.; Lu, Z. Y.; Zou, X. M.; Liao, L.; Shi, S. X.; Chen, P. P.; Fan, Z. Y.; Ho, J. C.; Li, T. X.; Chen, X. S.; Lu, W. *ACS Nano* **2014**, *8*, 3628–3635.

(22) Dufaux, T.; Burghard, M.; Kern, K. *Nano Lett.* **2012**, *12*, 2705–9.

(23) Wei, T.-Y.; Huang, C.-T.; Hansen, B. J.; Lin, Y.-F.; Chen, L.-J.; Lu, S.-Y.; Wang, Z. L. *Appl. Phys. Lett.* **2010**, *96*, 013508.

(24) Wallentin, J.; Wickert, P.; Ek, M.; Gustafsson, A.; Reine Wallenberg, L.; Magnusson, M. H.; Samuelson, L.; Deppert, K.; Borgström, M. T. *Appl. Phys. Lett.* **2011**, *99*, 253105.

(25) Cai, J.; Jie, J.; Jiang, P.; Wu, D.; Xie, C.; Wu, C.; Wang, Z.; Yu, Y.; Wang, L.; Zhang, X.; Peng, Q.; Jiang, Y. *Phys. Chem. Chem. Phys.* **2011**, *13*, 14663–7.

(26) Li, F.-Z.; Luo, L.-B.; Yang, Q.-D.; Wu, D.; Xie, C.; Nie, B.; Jie, J.-S.; Wu, C.-Y.; Wang, L.; Yu, S.-H. *Adv. Energy Mater.* **2013**, *3*, 579–583.

(27) Ren, P.; Hu, W.; Zhang, Q.; Zhu, X.; Zhuang, X.; Ma, L.; Fan, X.; Zhou, H.; Liao, L.; Duan, X.; Pan, A. *Adv. Mater.* **2014**, *26*, 7444–9.

(28) Guo, P.; Hu, W.; Zhang, Q.; Zhuang, X.; Zhu, X.; Zhou, H.; Shan, Z.; Xu, J.; Pan, A. *Adv. Mater.* **2014**, *26*, 2844–9.

(29) Chen, G.; Liang, B.; Liu, Z.; Yu, G.; Xie, X.; Luo, T.; Xie, Z.; Chen, D.; Zhu, M.-Q.; Shen, G. *J. Mater. Chem. C* **2014**, *2*, 1270–1277.

(30) Wang, J.; Gudiksen, M. S.; Duan, X.; Cui, Y.; Lieber, C. M. *Science* **2001**, *293*, 1455–7.

(31) Jain, V.; Nowzari, A.; Wallentin, J.; Borgström, M. T.; Messing, M. E.; Asoli, D.; Graczyk, M.; Witzigmann, B.; Capasso, F.; Samuelson, L.; Pettersson, H. *Nano Res.* **2014**, *7*, 544–552.

(32) Heo, K.; Lee, H.; Park, Y.; Park, J.; Lim, H.-J.; Yoon, D.; Lee, C.; Kim, M.; Cheong, H.; Park, J.; Jian, J.; Hong, S. *J. Mater. Chem.* **2012**, *22*, 2173–2179.

(33) Zhu, L.; Feng, C.; Li, F.; Zhang, D.; Li, C.; Wang, Y.; Lin, Y.; Ruan, S.; Chen, Z. *RSC Adv.* **2014**, *4*, 61691–61697.

(34) Ma, R. M.; Dai, L.; Huo, H. B.; Xu, W. J.; Qin, G. G. *Nano Lett.* **2007**, *7*, 3300–3304.

(35) Miao, J.; Hu, W.; Guo, N.; Lu, Z.; Liu, X.; Liao, L.; Chen, P.; Jiang, T.; Wu, S.; Ho, J. C.; Wang, L.; Chen, X.; Lu, W. *Small* **2015**, *11*, 936–42.

DOI: 10.1021/acs.nanolett.6b00104
Nano Lett. 2016, 16, 2548–2555

(36) Li, L.; Wu, P.; Fang, X.; Zhai, T.; Dai, L.; Liao, M.; Koide, Y.; Wang, H.; Bando, Y.; Golberg, D. *Adv. Mater.* **2010**, *22* (29), 3161−5.
(37) Gong, X.; Tong, M. H.; Xia, Y. J.; Cai, W. Z.; Moon, J. S.; Cao, Y.; Yu, G.; Shieh, C. L.; Nilsson, B.; Heeger, A. J. *Science* **2009**, *325*, 1665−1667.
(38) Manders, J. R.; Lai, T.-H.; An, Y.; Xu, W.; Lee, J.; Kim, D. Y.; Bosman, G.; So, F. *Adv. Funct. Mater.* **2014**, *24*, 7205−7210.
(39) For instance, common GaAs biased photodetector (400−900 nm) has responsivity of 0.45 A W^{-1} at 850 nm. http://search.newport.com/?q=*&x2=sku&q2=818-BB-45.
(40) Li, T.; Du, G.; Zhang, B.; Zeng, Z. *Appl. Phys. Lett.* **2014**, *105*, 093107.
(41) Sun, M. H.; Joyce, H. J.; Gao, Q.; Tan, H. H.; Jagadish, C.; Ning, C. Z. *Nano Lett.* **2012**, *12*, 3378−84.
(42) Zou, X.; Liu, X.; Wang, C.; Jiang, Y.; Wang, Y.; Xiao, X.; Ho, J. C.; Li, J.; Jiang, C.; Xiong, Q.; Liao, L. *ACS Nano* **2013**, *7*, 804−810.
(43) Storm, K.; Nylund, G.; Borgstrom, M.; Wallentin, J.; Fasth, C.; Thelander, C.; Samuelson, L. *Nano Lett.* **2011**, *11*, 1127−30.
(44) Lipatov, A.; Sharma, P.; Gruverman, A.; Sinitskii, A. *ACS Nano* **2015**, *9*, 8089−8098.
(45) Van, N. H.; Lee, J. H.; Sohn, J. I.; Cha, S.; Whang, D.; Kim, J. M.; Kang, D. J. *Nanotechnology* **2014**, *25*, 205201.
(46) Jena, D.; Konar, A. *Phys. Rev. Lett.* **2007**, *98* (13), 136805.
(47) Wang, X.; Wang, P.; Wang, J.; Hu, W.; Zhou, X.; Guo, N.; Huang, H.; Sun, S.; Shen, H.; Lin, T.; Tang, M.; Liao, L.; Jiang, A.; Sun, J.; Meng, X.; Chen, X.; Lu, W.; Chu, J. *Adv. Mater.* **2015**, *27*, 6575−6581.
(48) Lopez-Sanchez, O.; Lembke, D.; Kayci, M.; Radenovic, A.; Kis, A. *Nat. Nanotechnol.* **2013**, *8*, 497−501.
(49) Zhang, C.; Xu, Z.; Tian, W.; Tang, D. M.; Wang, X.; Bando, Y.; Fukata, N.; Golberg, D. *Nanotechnology* **2015**, *26*, 154001.
(50) Choi, W.; Cho, M. Y.; Konar, A.; Lee, J. H.; Cha, G. B.; Hong, S. C.; Kim, S.; Kim, J.; Jena, D.; Joo, J.; Kim, S. *Adv. Mater.* **2012**, *24*, 5832.
(51) Soci, C.; Zhang, A.; Xiang, B.; Dayeh, S. A.; Aplin, D. P. R.; Park, J.; Bao, X. Y.; Lo, Y. H.; Wang, D. *Nano Lett.* **2007**, *7*, 1003−1009.
(52) Das, K.; Mukherjee, S.; Manna, S.; Ray, S. K.; Raychaudhuri, A. K. *Nanoscale* **2014**, *6*, 11232−9.
(53) Konstantatos, G.; Sargent, E. H. *Nat. Nanotechnol.* **2010**, *5*, 391−400.
(54) Li, Q. G.; Penner, R. M. *Nano Lett.* **2005**, *5*, 1720−1725.
(55) Jeon, S.; Ahn, S. E.; Song, I.; Kim, C. J.; Chung, U. I.; Lee, E.; Yoo, I.; Nathan, A.; Lee, S.; Robertson, J.; Kim, K. *Nat. Mater.* **2012**, *11*, 301−5.
(56) Ma, R. M.; Dai, L.; Huo, H. B.; Yang, W. Q.; Qin, G. G.; Tan, P. H.; Huang, C. H.; Zheng, J. *Appl. Phys. Lett.* **2006**, *89*, 203120.
(57) Dai, Y.; Wu, P.; Dai, L.; Fang, X.; Qin, G. *J. Mater. Chem.* **2011**, *21*, 2858.

DOI: 10.1021/acs.nanolett.6b00104
Nano Lett. 2016, 16, 2548−2555